Journal of Intelligent & Robotic Systems (2018) 92:671–684
https://doi.org/10.1007/s10846-018-0774-z

Robust State and Output Feedback Control of Launched MAVs with Unknown Varying External Loads

Jinglan Li[1] · **Qinmin Yang**[1] · **Youxian Sun**[1]

Received: 13 July 2017 / Accepted: 10 January 2018 / Published online: 25 January 2018

Abstract
The operation of launched micro aerial vehicles (MAVs) with coaxial rotors is usually subject to unknown varying external disturbance. In this paper, a robust controller is designed to reject such uncertainties and track both position and orientation trajectories. A complete dynamic model of coaxial-rotor MAV is firstly established. When all system states are available, a nonlinear state-feedback control law is proposed based on feedback linearization and Lyapunov analysis. Further, to overcome the practical challenge that certain states are not measurable, a high gain observer is introduced to estimate unavailable states and an output feedback controller is developed. Rigid theoretical analysis verifies the stability of the entire closed-loop system. Additionally, extensive simulation studies have been conducted to validate the feasibility of the proposed scheme.

Keywords Coaxial-rotor micro aerial vehicles · Robust control · Filtered tracking errors · Lyapunov method · Nonlinear control

1 Introduction

Growing attention has been paid to mini or micro aerial vehicles (MAVs) along with the development of advanced techniques in recent years [10, 11, 16, 23, 25, 30]. Thanks to their features of small size, low cost and high efficiency of unmanned autonomy, MAVs have been recognized as new approaches to accomplish many tasks, such as homeland security protection, limited environment monitoring and battlefield assessment in both civilian and military applications [1, 8, 9, 22]. However, their applicability is still hindered by the low flight speed and limited cruising ability, especially in certain circumstances that rapid arrival to the destination is needed. To meet this requirement, a new type of unmanned Coaxial-Rotor MAVs (CRMAV) known as Gun Launched Micro Aerial Vehicle (GLMAV) are introduced by French-German Research Institute of Saint-Louis (ISL) [6].

✉ Qinmin Yang
qmyang@zju.edu.cn

[1] State Key Laboratory of Industrial Control Technology and the College of Control Science and Engineering, Zhejiang University, Hangzhou, Zhejiang 310027, China

A GLMAV is conceived as a kind of micro rotorcrafts with an architecture of two coaxial contra-rotating rotors. In its initial flight phase, a GLMAV stands like a projectile with its rotors folded into a shell. With the help of a gun-like delivery device, it can be quickly brought to the target zone. Once arriving at the apogee, the rotors are deployed and start rotating to slow down the projectile for the hovering flight as a MAV. Finally, it can make a return voyage after fulfilling missions. For autonomous operations, a GLMAV has to be equipped with a navigation system like GPS, a power system, and an autopilot for control purposes. Other devices such as vision systems can also be equipped for meeting mission requirements.

Early research efforts have been devoted to verification of designs [6] (e.g., two coaxial contra-rotating rotors architecture, size confirmation, and payload calculation), and modeling the dynamics of a GLMAV during hovering flights via both theoretical and experimental studies [15]. Besides, aerodynamic modeling and parameters identifications [12–14] have also been carried out to complete the dynamic 6 DOF model of a GLMAV.

Numerous attempts have also been made from the perspective of control design. A standard nonlinear backstepping based tracking control strategy is proposed in [3] to enforce desired trajectories of the GLMAV. However, the

effect of unknown external wind still can not be well handled by the proposed control law. Moreover, adaptive controls have also been discussed to deal with unknown aerodynamic effects [4, 5]. The external forces and moments are estimated online for control purpose. But only constant or slowly time-varying unknown disturbances are considered in simulation tests. Recent advances also include observers (i.e., a liner extended state observer (LESO) and a disturbance observer with finite time convergence (FTDO)) to solve the path tracking problem of a GLMAV despite of unknown aerodynamic effects [20, 21]. The controllers are able to deliver satisfactory performance under a sine-like external disturbance. However, most aforementioned solutions are based on backstepping methodology, which may lead to a time-scale separation [28, 29] or extreme ill conditions of the control problem, since the derivative of the control signal enters into the remaining system [17]. Moreover, one of the widely recognized drawbacks of the backstepping design is that the complexity of the system increases drastically with the system order resulting from the repeated differentiation of the virtual control input [19].

Therefore, the focus of this paper is to provide a high-performance backstepping-free trajectory tracking control strategy for a GLMAV. A mathematical model for control design is firstly derived in hovering flight. Subsequently, an error dynamics based on filtered tracking error is developed, and a nonlinear feedback linearization based control law is discussed. A robust design is introduced to deal with unknown time-varying external disturbance. The disadvantages involved by backstepping method are avoided. Moreover, considering that certain system states are not available, an output feedback control version is designed with the help of a high-gain observer. The tracking performance along with the stability of the entire closed-loop system in the presence of unknown time-varying loads is guaranteed via strict Lyapunov analysis.

The rest of this paper is organized as follows: Section 2 discusses modeling of a GLMAV dynamics, while Section 3 presents the procedures of the control law design and the stability analyzes based on Lyapunov theory. Simulation studies are conducted in Sections 4 and 5 concludes the work accomplished in this paper.

2 System Modeling

In this section, an explicit outline of the 6 DOF GLMAV dynamics in hovering fight is introduced. The complete model of GLMAV can be divided into two subsystems: a rigid body model and an aerodynamic model [7]. The reference frames and major modeling parameters considered in this study are diagrammatically shown in Fig. 1.

2.1 Rigid Body Model

An inertial frame $\{O, x_e, y_e, z_e\}$ and a body-fixed frame $\{G, x_b, y_b, z_b\}$ are firstly defined for the transformation of position, velocity, angles and angular rates [18]. By reasonably considering the GLMAV to be a rigid body with a fixed mass m, its translational and rotational dynamics can be derived by applying Newton-Euler laws based on a 6 DOF model. Therefore, the dynamic model of the GLMAV with respect to the inertial frame can be given by

$$\begin{aligned} \dot{p} &= v \\ \dot{v} &= a \\ ma &= R_\eta f \\ J\dot{\omega} &= -\omega \times J\omega + \Gamma \end{aligned} \tag{1}$$

where $p, v, a \in \mathbb{R}^3$ are the position, linear velocity and acceleration of the center of mass G with regard to the reference point O in the initial frame. $f, \Gamma \in \mathbb{R}^3$ are the total forces and moments that act on the vehicle in body-fixed frame, $\omega \in \mathbb{R}^3$ is the angular velocity, $J = \text{diag}[J_{xx}, J_{yy}, J_{zz}] \in \mathbb{R}^{3\times3}$ is the diagonal initial matrix, and $R_\eta \in \mathbb{R}^{3\times3}$ is the rotation matrix from the body frame to the initial frame, which is a function of the Euler angle set $\eta = [\phi, \theta, \psi]^T \in \mathbb{R}^3$

$$R_\eta = \begin{bmatrix} c_\theta c_\psi & s_\phi s_\theta c_\psi - c_\phi s_\psi & c_\phi s_\theta c_\psi + s_\phi s_\psi \\ c_\theta s_\psi & s_\phi s_\theta s_\psi + c_\phi c_\psi & c_\phi s_\theta s_\psi - s_\phi c_\psi \\ -s_\theta & s_\phi c_\theta & c_\phi c_\theta \end{bmatrix} \tag{2}$$

where ϕ, θ and ψ are the roll, pitch and yaw angles, respectively. For convenience, define $s_\eta = \sin\eta$, $c_\eta = \cos\eta$, $t_\eta = \tan\eta$. Finally, the attitude dynamics derived by Euler's law in body-fixed frame can be also given by

$$\dot{\eta} = Q_\eta \omega \tag{3}$$

with

$$Q_\eta = \begin{bmatrix} 1 & s_\phi t_\theta & c_\phi t_\theta \\ 0 & c_\phi & -s_\phi \\ 0 & s_\phi/c_\theta & c_\phi/c_\theta \end{bmatrix} \tag{4}$$

2.2 Aerodynamic Model

During flight in outdoor environment, the dynamics of GLMAV is subject to various aerodynamic forces and moments. By neglecting the gyroscopic effect on moments, the major loads usually considered are generated by the coaxial rotors, the cyclic swashplate incidence angles, and the airflow [15]. Therefore, the motion of GLMAV is the

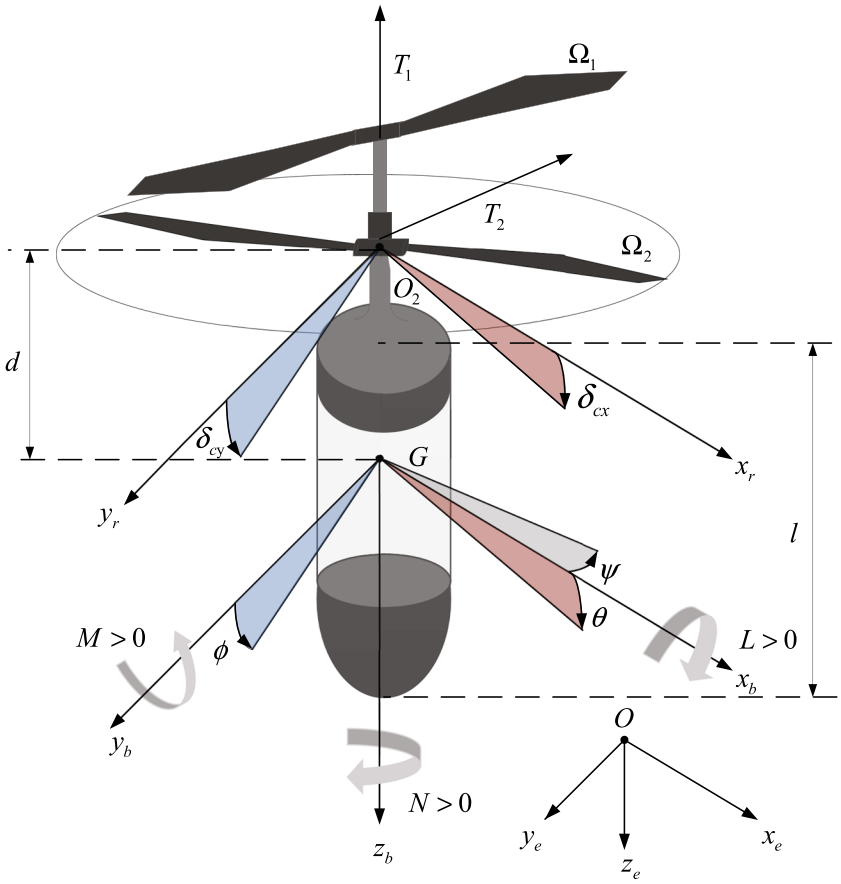

Fig. 1 Reference frames and parameters of GLMAV

result of thrusts generated by rotors, aerodynamic forces induced by wind speed, gravitational force.

2.2.1 Forces Generated by Rotors

Thrusts are generated by the upper rotor T_1 and the lower one T_2. Both two rotors contribute to the vertical force, which can be employed by the GLMAV to control the rate of climb. Moreover, the lower rotor can produce two lateral forces owing to the swashplate incidence angles.

Theoretically, the total rotor thrust T is the vector sum of T_1 and T_2. However, provided that there commonly exists an aerodynamic coefficient loss in vertical direction due to the airflow interactions, the total thrust is calculated as [15]

$$T = \begin{bmatrix} T_x \\ T_y \\ T_z \end{bmatrix} = \begin{bmatrix} -\beta \sin \delta_{c_y} \cos \delta_{c_x} \Omega_2^2 \\ -\beta \sin \delta_{c_x} \Omega_2^2 \\ \sigma \alpha \Omega_1^2 + \sigma \beta \cos \delta_{c_x} \cos \delta_{c_y} \Omega_2^2 \end{bmatrix} \tag{5}$$

where Ω_1 and Ω_2 are the rotor rotation speeds of the upper rotor and the lower rotor, α and β are the corresponding aerodynamic coefficients, δ_{c_x} and δ_{c_y} are the swashplate incidence angles and σ is an efficiency coefficient with $0.8 \leq \sigma \leq 1$.

2.2.2 Forces Acting on the Body

Two major forces acting on the body of a GLMAV are considered: the aerodynamic force f_w induced by wind speed, and the gravity f_g.

First, the aerodynamic force f_w directly results from the total wind speed V, which mainly contains the airflow speed V_r generated by the rotors, the body velocity V_b generated by the GLMAV's motion, and the external wind V_w which is usually unknown [3]. Thus, the total wind speed in body-fixed frame becomes

$$V = V_r - V_b + V_w = \begin{bmatrix} V_x \\ V_y \\ V_z \end{bmatrix} \tag{6}$$

Therefore, f_w can be determined by

$$f_w = \begin{bmatrix} f_{w_x} \\ f_{w_y} \\ f_{w_z} \end{bmatrix} = \begin{bmatrix} \frac{1}{2} \rho S_c C_x V_x \| V \| \\ \frac{1}{2} \rho S_c C_y V_y \| V \| \\ \frac{1}{2} \rho S_s C_z V_z \| V \| \end{bmatrix} \tag{7}$$

where S_c is the cylinder surface, S_s the half-sphere surface, and C_x, C_y, C_z the aerodynamic coefficients.

The gravity of a GLMAV in the body-fixed frame can be written as

$$f_g = mg \begin{bmatrix} -\sin\theta \\ \cos\theta \sin\phi \\ \cos\theta \cos\phi \end{bmatrix} = R_\eta^T \begin{bmatrix} 0 \\ 0 \\ mg \end{bmatrix} \tag{8}$$

Generally, the aerodynamic force f_w is difficult to identify in practice, and thus it is regarded as the unknown external disturbance acting on the body of a GLMAV, which is compactly denoted by $f_{ext} = f_w$ in the body frame, or F_{ext} in the inertial frame, such that $F_{ext} = R_\eta f_{ext}$.

Thus, the total force can be now given as

$$f = T + f_g + f_{ext} \tag{9}$$

2.2.3 Moments Acting on the Body

In this study, the major moment acting on the body of a GLAMV is considered to be induced by the rotors. As a result, the roll moment L and the pith moment M produced by the longitudinal and lateral tilts of swashplate can be presented as a cross product of the distance vector from the gravity center G to the lower rotor rotation center O_2 and the lower rotor thrust. Meanwhile, the yaw moment depends on the speed difference between the two rotors and the yaw aerodynamic coefficients. Therefore, the moment vector can be given as

$$\tau = \begin{bmatrix} L \\ M \\ N \end{bmatrix} = \begin{bmatrix} -d\beta \sin\delta_{c_x} \Omega_2^2 \\ d\beta \sin\delta_{c_y} \cos\delta_{c_x} \Omega_2^2 \\ \gamma_1 \Omega_1^2 + \gamma_2 \Omega_2^2 \end{bmatrix} \tag{10}$$

where d is the distance between center poins G and O_2, γ_1, γ_2 the yaw aerodynamic coefficients.

Similarly, by considering an unknown external moment M_{ext} resulted from the unknown forces in the body frame, the total moments acting on the GLMAV are summarized as

$$\Gamma = \tau + M_{ext} \tag{11}$$

2.3 System Dynamics

Provided that the contribution of lateral forces induced by the incidence angles of the swashplate is negligible compared to the main vertical force T_z, the lateral forces T_x and T_y in Eq. 5 are both omitted for simplicity [5], or T_x=T_y=0. Hence, the forces acting on the GLMAV are simplified as

$$f = T_z e_3 + R_\eta^T mg e_3 + f_{ext} \tag{12}$$

with $e_3 = [0, 0, 1]^T$.

Thus, the dynamics for control design can be rewritten as

$$\begin{aligned} \dot{p} &= v \\ \dot{v} &= \tfrac{1}{m}\left(T_z R_\eta e_3 + mg e_3 + F_{ext}\right) \\ \dot{\eta} &= Q_\eta \omega \\ \dot{\omega} &= J^{-1}(-\omega \times J\omega + \tau + M_{ext}) \end{aligned} \tag{13}$$

In this study, T_z and τ are regarded as the control inputs of the GLMAV system. Once T_z and τ are determined by certain control law, the four actual control signals Ω_1, Ω_2, δ_{c_x} and δ_{c_y} acting on the GLMAV can be readily calculated. As a matter of fact, by considering that the swashplate incidence angles are small enough, paraxial approximation is applicable [27], such that $sin\zeta \approx \zeta$, $cos\zeta \approx 1$. Thus, the following relationship can be established by recalling Eqs. 5 and 10.

$$\begin{aligned} \Omega_1^2 &= \tfrac{T_z - \sigma\beta\Omega_2^2}{\sigma\alpha} \\ \Omega_2^2 &= \tfrac{\sigma\alpha N - \gamma_1 T_z}{\sigma\alpha\gamma_2 - \sigma\beta\gamma_1} \\ \delta_{c_x} &= \tfrac{-L}{d\beta\Omega_2^2} \\ \delta_{c_y} &= \tfrac{M}{d\beta\Omega_2^2} \end{aligned} \tag{14}$$

Remark 1 It has to be noted that the un-modeled disturbances F_{ext} and M_{ext} are assumed to be time-varying functions, instead of constants in literature [4, 24]. They will be compensated by the robust control design introduced in the following section.

3 Control Design

In this section, a robust controller is proposed for trajectory tracking of GLMAV based on Lyapunov method. The objective is to manipulate the GLMAV (13) to track a desired translational and rotational trajectory, or equivalently, to track a desired position $p_d = [x_d, y_d, z_d]^T$ and a desired yaw angle ψ_d. The whole diagram of the closed-loop control system is shown in Fig. 2. Before proceeding, following mild assumptions are present.

Assumption 1 *The unknown disturbances M_{ext}, and F_{ext}, along with the first-order and second-order derivatives are bounded, such that $|M_{ext}| \le \bar{M}$, $|F_{ext}| \le \bar{F}_0$, $|\dot{F}_{ext}| \le \bar{F}_1$, $|\ddot{F}_{ext}| \le \bar{F}_2$, where $|\cdot|$ denotes the L_1-norm.*

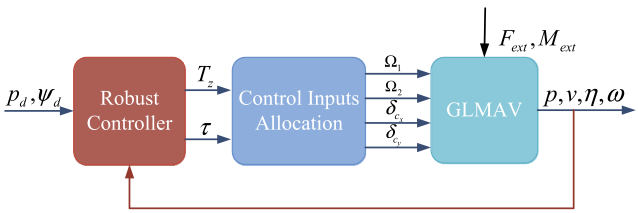

Fig. 2 Diagram of the closed-loop control system of GLMAV

Assumption 2 *The desired posture* $p_d = [x_d, y_d, z_d]^T$ *and* ψ_d *are smooth and bounded along with their derivatives.*

3.1 Filtered Tracking Error Dynamics

Firstly, the position tracking error δ_{p_0} is defined as

$$\delta_{p_0} = p - p_d \tag{15}$$

Then, the filtered position tracking error is defined as

$$r_p = k_{p0}\delta_{p_0} + k_{p_1}\delta_{p_1} + k_{p_2}\delta_{p_2} + \delta_{p_3} \tag{16}$$

whose derivative can be derived as

$$\dot{r}_p = k_{p0}\delta_{p_1} + k_{p_1}\delta_{p_2} + k_{p_2}\delta_{p_3} + \delta_{p_4} \tag{17}$$

with $\dot{\delta}_{p_0} = \delta_{p_1}$, $\dot{\delta}_{p_1} = \delta_{p_2}$, $\dot{\delta}_{p_2} = \delta_{p_3}$, $\dot{\delta}_{p_3} = \delta_{p_4}$ and k_{p_0}, $k_{p_1}, k_{p_2} \in \mathbb{R}^+$ are positive constants to meet that $s^3 + k_{p_2} s^2 + k_{p_1} s + k_{p_0}$ is Hurwitz. Thus, $\delta_{p_i} \to 0$ asymptotically as $r_p \to 0$.

By differentiating δ_{p_0} and recalling the system dynamics (13), one has

$$\begin{aligned} \delta_{p_1} &= v - \dot{p}_d \\ \delta_{p_2} &= \tfrac{1}{m}(T_z R_\eta e_3 + mge_3 + F_{ext}) - \ddot{p}_d \\ \delta_{p_3} &= \tfrac{1}{m}\left(\dot{T}_z R_\eta e_3 + T_z R_\eta \tilde{\omega} e_3 + \dot{F}_{ext}\right) - p_d^{(3)} \end{aligned} \tag{18}$$

where $R_\eta \tilde{\omega} = \dot{R}_\eta$ with $\tilde{\omega}$ being a skew symmetric matrix of the vector ω as

$$\tilde{\omega} = \begin{bmatrix} 0 & -\omega_z & \omega_y \\ \omega_z & 0 & -\omega_x \\ -\omega_y & \omega_x & 0 \end{bmatrix} \tag{19}$$

Proceeding with differentiating δ_{p_3} and recalling Eq. 13 yield

$$\begin{aligned} \delta_{p_4} = \tfrac{1}{m}\big(&\ddot{T}_z R_\eta e_3 - T_z R_\eta \tilde{e}_3 J^{-1}\tau + 2\dot{T}_z R_\eta \tilde{\omega} e_3 \\ &+ T_z R_\eta \tilde{\omega}^2 e_3 + T_z R_\eta \tilde{e}_3 J^{-1}(\omega \times J\omega - M_{ext})\big) \\ &+ \tfrac{\ddot{F}_{ext}}{m} - p_d^{(4)} \end{aligned} \tag{20}$$

where $\tilde{e}_3$ is the skew symmetric matrix of the vector e_3 as

$$\tilde{e}_3 = \begin{bmatrix} 0 & -1 & 0 \\ 1 & 0 & 0 \\ 0 & 0 & 0 \end{bmatrix} \tag{21}$$

Similarly, the orientation tracking error δ_{ψ_0} is defined as

$$\delta_{\psi_0} = \psi - \psi_d = e_3^T \eta - \psi_d \tag{22}$$

Subsequently, the filtered orientation tracking error and its derivative can be defined as

$$r_\psi = k_{\psi_0}\delta_{\psi_0} + \delta_{\psi_1} \tag{23}$$

$$\dot{r}_\psi = k_{\psi_0}\delta_{\psi_1} + \delta_{\psi_2} \tag{24}$$

with $\dot{\delta}_{\psi_0} = \delta_{\psi_1}$, $\dot{\delta}_{\psi_1} = \delta_{\psi_2}$ and k_{ψ_0} being a positive constant. Thus, $\delta_{\psi_i} \to 0$ asymptotically as $r_\psi \to 0$.

Recalling Eq. 13, the first-order and second-order derivatives of the orientation tracking error δ_{ψ_0} can be calculated as

$$\delta_{\psi_1} = e_3^T Q_\eta \omega - \dot{\psi}_d \tag{25}$$

$$\begin{aligned} \delta_{\psi_2} = e_3^T \left(\dot{Q}_\eta \omega + Q_\eta J^{-1}(-\omega \times J\omega + \tau + M_{ext})\right) \\ - \ddot{\psi}_d \end{aligned} \tag{26}$$

3.2 State Feedback Control Design

It is firstly assumed that all states of the GLMAV system are available for control design as feedback signals, i.e, p, v, a, $\dot{a}$, η, ω are all accessible. In this way, a state feedback control design is developed in this subsection.

The objective of the controller is to achieve $r_p \to 0$ and $r_\psi \to 0$. Firstly, substituting Eqs. 18 and 20 into Eq. 17 yields

$$\begin{aligned} \dot{r}_p = k_{p_0}\delta_{p_1} + k_{p_1}\delta_{p_2} + k_{p_2}\delta_{p_3} - p_d^{(4)} + \tfrac{\ddot{F}_{ext}}{m} \\ + \tfrac{1}{m}\big(\ddot{T}_z R_\eta e_3 - T_z R_\eta \tilde{e}_3 J^{-1}\tau + 2\dot{T}_z R_\eta \tilde{\omega} e_3 \\ + T_z R_\eta \tilde{\omega}^2 e_3 + T_z R_\eta \tilde{e}_3 J^{-1}(\omega \times J\omega - M_{ext})\big) \end{aligned} \tag{27}$$

Thus, if the control law for position tracking is designed to satisfy

$$\begin{aligned} &\tfrac{1}{m}\left(\ddot{T}_z R_\eta e_3 - T_z R_\eta \tilde{e}_3 J^{-1}\tau\right) \\ &= -\tfrac{1}{m}\left(2\dot{T}_z R_\eta \tilde{\omega} e_3 + T_z R_\eta \tilde{\omega}^2 e_3 + T_z R_\eta \tilde{e}_3 J^{-1}(\omega \times J\omega)\right) \\ &\quad -\mathrm{sgn}(r_p)\Theta_p - c_p r_p - \left(k_{p_0}\delta_{p_1} + k_{p_1}\delta_{p_2} + k_{p_2}\delta_{p_3}\right) + p_d^{(4)} \end{aligned} \tag{28}$$

one has the dynamics of the filtered position tracking error as

$$\dot{r}_p = -c_p r_p - \mathrm{sgn}(r_p)\Theta_p + \Phi_p \tag{29}$$

where c_p is an user-defined positive constant,

$$\Theta_p = \frac{1}{m}\left(|T_z R_\eta \tilde{e}_3 J^{-1}|\bar{M} + \bar{F}_2\right)$$

and

$$\Phi_p = \frac{1}{m}\left(-T_z R_\eta \tilde{e}_3 J^{-1} M_{ext} + \ddot{F}_{ext}\right).$$

Furthermore, the dynamics of the filtered orientation tracking error can be obtained by combining Eqs. 24 – 26 as

$$\begin{aligned} \dot{r}_\psi = k_{\psi_0}\delta_{\psi_1} - \ddot{\psi}_d + e_3^T Q_\eta J^{-1}\tau \\ + e_3^T\left(\dot{Q}_\eta \omega + Q_\eta J^{-1}(-\omega \times J\omega + M_{ext})\right) \end{aligned} \tag{30}$$

Similarly, design the control law for orientation tracking to satisfy

$$\begin{aligned} e_3^T Q_\eta J^{-1}\tau = e_3^T\left(-\dot{Q}_\eta \omega + Q_\eta J^{-1}(\omega \times J\omega)\right) \\ -\mathrm{sgn}(r_\psi)\Theta_\psi - c_\psi r_\psi - k_{\psi_0}\delta_{\psi_1} + \ddot{\psi}_d \end{aligned} \tag{31}$$

which give us the dynamics of the orientation position tracking error as

$$\dot{r}_\psi = -c_\psi r_\psi - \mathrm{sgn}\left(r_\psi\right)\Theta_\psi + \Phi_\psi \tag{32}$$

where c_ψ is an user-defined positive constant, $\Theta_\psi = |e_3^T Q_\eta J^{-1}|\bar{M}$, and $\Phi_\psi = e_3^T Q_\eta J^{-1} M_{ext}$.

Therefore, Combining Eqs. 28 and 31, the two control inputs can be compactly obtained by

$$\begin{bmatrix} \tau \\ \ddot{T}_z \end{bmatrix} = C^{-1}X = \begin{bmatrix} C_{11} & C_{12} \\ C_{21} & C_{22} \end{bmatrix}^{-1} \begin{bmatrix} X_1 \\ X_2 \end{bmatrix} \tag{33}$$

with

$$\begin{aligned} X_1 = & -\tfrac{1}{m}\left(2\dot{T}_z R_\eta \tilde{\omega} e_3 + T_z R_\eta \tilde{\omega}^2 e_3 \right. \\ & \left. + T_z R_\eta \tilde{e}_3 J^{-1}(\omega \times J\omega)\right) - \mathrm{sgn}(r_p)\Theta_p - c_p r_p \\ & -(k_{p_0}\delta_{p_1} + k_{p_1}\delta_{p_2} + k_{p_2}\delta_{p_3}) + p_d^{(4)} \\ X_2 = & \; e_3^T\left(-\dot{Q}_\eta \omega + Q_\eta J^{-1}(\omega \times J\omega)\right) \\ & -\mathrm{sgn}\left(r_\psi\right)\Theta_\psi - c_\psi r_\psi - k_{\psi_0}\delta_{\psi_1} + \ddot{\psi}_d \\ C_{11} = & -\tfrac{1}{m} T_z R_\eta \tilde{e}_3 J^{-1} \\ C_{12} = & \tfrac{1}{m} R_\eta e_3 \\ C_{21} = & \; e_3^T Q_\eta J^{-1} \\ C_{22} = & \; 0 \end{aligned} \tag{34}$$

Remark 2 It should be noted that the position tracking controller is based on establishing a dynamics of T_z, and $\ddot{T}_z$ is employed as the augmented control signal. The vertical thrust T_z and its first derivative $\dot{T}_z$ are considered as the internal states of the controller and employed as feedback.

Remark 3 The matrix C in Eq. 33 must be invertible for the acquirement of the control inputs, the determinant of which can be calculated as

$$\det(C) = -\frac{1}{m^3}\frac{1}{J_{xx}J_{yy}J_{zz}} T_z^2 \frac{\cos\phi}{\cos\theta} \tag{35}$$

It is straightforward to find that there exist two "failure situations", in which $\det(C) = 0$: 1) The vertical thrust equals to zero; 2) The GLMAV is overturned [3]. In this study, the desired posture is designed to avoid the two scenarios and thus they are out of the scope of discussion.

Finally, the stability analysis for the control laws designed in Eqs. 33 and 34 can be given by the following theorem.

Theorem 1 *Let Assumptions 1 and 2 hold. Consider a GLMAV system represented by Eq. 13 with the state vector available. If the controller is designed as Eq. 33, then, all system signals are bounded, and the tracking errors converge to zero asymptotically, i.e.,* $\delta_{p_0} \to 0$, $\delta_{\psi_0} \to 0$, *as* $t \to \infty$.

Proof Please see the Appendix. □

3.3 Output Feedback Control Design with High-Gain Observer

In practice, not all states of the GLMAV system are available. In general, only the position states p, v and the attitude states η, ω are accessible for feedback. As a consequence, the state-feedback based controller designed in the previous subsection cannot be directly implemented. In this case, a high-gain state observer is designed for estimating the unavailable states, whose outputs are subsequently routed to the controller.

Firstly, rewrite the system state δ_{p_4} in Eq. 20 as

$$\delta_{p_4} = \chi + \Phi_p \tag{36}$$

with

$$\begin{aligned} \chi = & \tfrac{1}{m}\left(\ddot{T}_z R_\eta e_3 - T_z R_\eta \tilde{e}_3 J^{-1}\tau\right) + \tfrac{1}{m}\left(2\dot{T}_z R_\eta \tilde{\omega} e_3 \right. \\ & \left. + T_z R_\eta \tilde{\omega}^2 e_3 + T_z R_\eta \tilde{e}_3 J^{-1}(\omega \times J\omega)\right) - p_d^{(4)} \end{aligned} \tag{37}$$

is a known function.

Subsequently, the structure of the high-gain observer to identify the unknown states δ_{p_2} and δ_{p_3} is shown as

$$\begin{aligned} \dot{\hat{\delta}}_{p_1} &= \hat{\delta}_{p_2} + h_1(\delta_{p_1} - \hat{\delta}_{p_1}) \\ \dot{\hat{\delta}}_{p_2} &= \hat{\delta}_{p_3} + h_2(\delta_{p_1} - \hat{\delta}_{p_1}) \\ \dot{\hat{\delta}}_{p_3} &= \chi + h_3(\delta_{p_1} - \hat{\delta}_{p_1}) \end{aligned} \tag{38}$$

where $\hat{\delta}_{p_1}$, $\hat{\delta}_{p_2}$, and $\hat{\delta}_{p_3}$ are respectively the estimate of δ_{p_1}, δ_{p_2} and δ_{p_3}. $h_1, h_2, h_3 \in \mathbb{R}^+$ are positive constant observer gains satisfying $1 \ll h_1 \ll h_2 \ll h_3$.

The observer errors are defined as $e_p = [e_{p_1}^T, e_{p_2}^T, e_{p_3}^T]^T$ with $e_{p_i} = \delta_{p_i} - \hat{\delta}_{p_i}$, $i = 1, 2, 3$. The error dynamics can be delivered from the definitions and Eq. 38 as

$$\begin{aligned} \dot{e}_{p_1} &= e_{p_2} - h_1 e_{p_1} \\ \dot{e}_{p_2} &= e_{p_3} - h_2 e_{p_1} \\ \dot{e}_{p_3} &= \Phi_p - h_3 e_{p_1} \end{aligned} \tag{39}$$

which can be compactly written as

$$\dot{e}_p = A e_p + B\Phi_p \tag{40}$$

with

$$A = \begin{bmatrix} -h_1 I_3 & I_3 & 0_3 \\ -h_2 I_3 & 0_3 & I_3 \\ -h_3 I_3 & 0_3 & 0_3 \end{bmatrix} \qquad B = \begin{bmatrix} 0_3 & 0_3 & I_3 \end{bmatrix}^T \tag{41}$$

where $I_3 \in \mathbb{R}^{3\times 3}$ is the identity matrix, and $0_3 \in \mathbb{R}^{3\times 3}$ is the null matrix. A is chosen to be a Hurwitz matrix, thus there exists a symmetric, positive definite matrix $P \in \mathbb{R}^{9\times 9}$ s.t.

$$A^T P + PA = -\lambda I_9 \tag{42}$$

where $\lambda \in \mathbb{R}^+$ is a positive constant, and $I_9 \in \mathbb{R}^{9\times 9}$ is the identify matrix.

Moreover, it has to be noted that the discontinuous function $\mathrm{sgn}(\cdot)$ in the control law (33) will require infinite

actuator bandwidth and result in chattering effects [31]. To overcome this difficulty, the following continuous hyperbolic function tanh(·) is employed instead to replace sgn(·), where

$$\tanh(u) = \frac{e^{u} - e^{-u}}{e^{u} + e^{-u}} \tag{43}$$

Following Lemma is then presented for stability analysis.

Lemma 1 *([26]) The following inequality holds for any constant $\varepsilon > 0$ and for any $u \in \mathbb{R}$*

$$0 \leq |u| - u \tanh\left(\frac{u}{\varepsilon}\right) \leq \kappa\varepsilon \tag{44}$$

where κ satisfies $\kappa = e^{-(\kappa+1)}$; i.e., $\kappa = 0.2785$.

Thereafter, provided that the estimates $\hat{\delta}_{p_2}$ and $\hat{\delta}_{p_3}$ are utilized to replace the unknown states δ_{p_2} and δ_{p_3}, the output feedback controller can be given as

$$\begin{bmatrix} \tau \\ \ddot{T}_z \end{bmatrix} = C^{-1}\overline{X} = \begin{bmatrix} C_{11} & C_{12} \\ C_{21} & C_{22} \end{bmatrix}^{-1} \begin{bmatrix} \overline{X}_1 \\ \overline{X}_2 \end{bmatrix} \tag{45}$$

with

$$\begin{aligned} \overline{X}_1 = & -\tfrac{1}{m}\left(2\dot{T}_z R_\eta \tilde{\omega} e_3 + T_z R_\eta \tilde{\omega}^2 e_3 \right. \\ & \left. + T_z R_\eta \tilde{e}_3 J^{-1}(\omega \times J\omega)\right) - \tanh\left(\tfrac{\hat{r}_p}{\varepsilon_p}\right)\Theta_p - c_p \hat{r}_p \\ & - \left(k_{p_0}\delta_{p_1} + k_{p_1}\hat{\delta}_{p_2} + k_{p_2}\hat{\delta}_{p_3}\right) + p_d^{(4)} \\ \overline{X}_2 = & \, e_3^T\left(-\dot{Q}_\eta \omega + Q_\eta J^{-1}(\omega \times J\omega)\right) \\ & - \tanh\left(\tfrac{r_\psi}{\varepsilon_\psi}\right)\Theta_\psi - c_\psi r_\psi - k_{\psi_0}\delta_{\psi_1} + \ddot{\psi}_d \end{aligned} \tag{46}$$

At last, the stability analysis for the output feedback control law designed in Eqs. 45 and 46 is given by the following theorem.

Theorem 2 *Let Assumptions 1 and 2 hold. Consider a GLMAV system represented by Eq. 13 with only the system states p, v, η and ω available. If an output feedback controller is designed as Eq. 45 with a state observer in Eq. 38, then, the tracking errors, as well as all system signals, are uniformly ultimately bounded (UUB). Moreover, the tracking errors can be arbitrarily reduced by increasing control gains.*

Proof Please see the Appendix. □

4 Simulation Results

In order to verify the performance of the proposed controller, extensive simulation studies are conducted on a complete GLMAV model in Eq. 1. The parameters adopted in simulations are tabulated in Table 1 [7]. A trajectory tracking task in a hovering flight is considered in this study, and the initial conditions are set as: $p_0 = [0 \quad 0 \quad 100]^T$, $v_0 = [0 \quad 0 \quad 0]^T$, $a_0 = [0 \quad 0 \quad 0]^T$, $\eta_0 = [0 \quad 0 \quad 0]^T$ and $\omega_0 = [0 \quad 0 \quad 0]^T$. For simplicity, only the output-feedback controller is implemented in simulation tests and the corresponding parameters of the controller are selected as $c_p = 2.5$, $k_{p_0} = 1.5$, $k_{p_1} = 2.5$, $k_{p_2} = 2.5$, $c_\psi = 2.5$, $k_{\psi_0} = 2.5$, $\bar{F}_2 = 5 \times 10^2$, $\bar{M} = 6 \times 10^{-3}$, $\varepsilon_p = 2 \times 10^2$, $\varepsilon_\psi = 2 \times 10^{-2}$, $h_1 = 50$, $h_2 = 500$ and $h_3 = 5000$.

Table 1 Parameters of GLMAV for simulations

Parameter	Value	Unit
α	-3.6835×10^{-5}	$N.rad^{-2}.s^{-2}$
β	-3.7760×10^{-5}	$N.rad^{-2}.s^{-2}$
γ_1	1.4765×10^{-6}	$N.m.rad^{-2}.s^{-2}$
γ_2	-1.3266×10^{-6}	$N.m.rad^{-2}.s^{-2}$
ρ	1.204	$kg.m^{-3}$
σ	1	–
C_x	0.09	–
C_y	0.09	–
C_z	0.2	–
d	67.6×10^{-3}	m
D	40×10^{-3}	m
g	9.81	$m.s^{-2}$
J_{xx}	1.383×10^{-3}	$kg.m^2$
J_{yy}	1.383×10^{-3}	$kg.m^2$
J_{zz}	2.72×10^{-4}	$kg.m^2$
l	130×10^{-3}	m
m	410×10^{-3}	kg
S_c	10.4×10^{-3}	m^2
S_{prop}	34×10^{-2}	m^2
S_s	5.0×10^{-3}	m^2

Firstly, the performance of the proposed controller is evaluated in four scenarios: 1) flight without external disturbance; 2) flight with sine-like external disturbance; 3) flight with sensing noise; 4) flight with turbulent disturbance. Initially, the MAV is supposed to run in the operational phase. It is maneuvered to track a piecewise continuous desired trajectory [2]. Additionally, a path tracking comparison study in opposite to [20, 21] has also been carried out to validate the benefits of the proposed scheme.

4.1 Scenario 1: Flight without External Disturbance

Firstly, consider an ideal case where no external disturbance is acting on the body of the GLMAV, i.e., $F_{ext}, M_{ext} = 0$. The position and orientation tracking performance of the proposed robust controller in hovering flight is illustrated

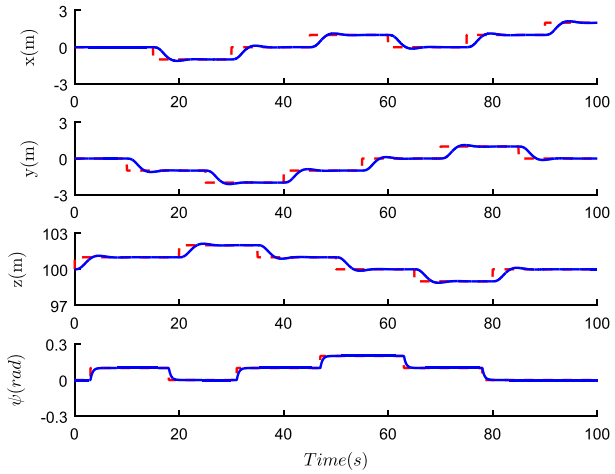

(a) System outputs x, y, z and ψ (solid line) and the desired trajectories x_d, y_d, z_d and ψ_d (dashed line).

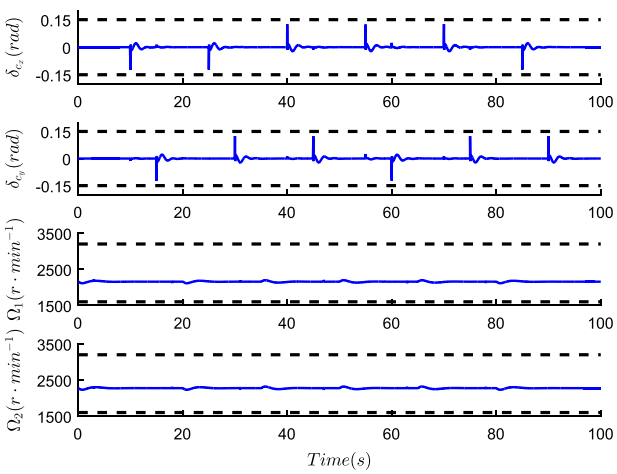

(b) Input signals δ_{c_x}, δ_{c_y}, Ω_1 and Ω_2 (solid line).

Fig. 3 Simulation result without external loads

in Fig. 3a. It can be found that the vehicle is able to converge to the desired curve with settling time of less than 5 seconds. Moreover, the trajectories of control inputs are also demonstrated in Fig. 3b, which shows the boundedness of control signals and the stability of the closed-loop system. Physical limits of the actuators for safe flights are also plotted as dashed lines.

4.2 Scenario 2: Flight with Sine-like External Disturbance

In practice, the MAV is usually subject to varying external disturbance. In this scenario, to verify the robustness of the proposed controller, consider unknown external loads F_{ext} and M_{ext} on the system dynamics during flight. Specifically, sine-like signals [20] are adopted in this case as following

$$\begin{aligned} F_{ext} &= \begin{bmatrix} 1+0.2\sin(0.5t) \\ 1+0.2\sin(0.5t) \\ 1+0.2\sin(0.5t) \end{bmatrix} (N) \\ M_{ext} &= \begin{bmatrix} 1.5+0.3\sin(0.5t) \\ 1.5+0.3\sin(0.5t) \\ 1.5+0.3\sin(0.5t) \end{bmatrix} (mN.m) \end{aligned} \tag{47}$$

The generated output trajectories of the proposed scheme are plotted in Fig. 4a. It can be observed that, when the proposed robust controller is enforced, the GLMAV's position and orientation still can rapidly track the desired

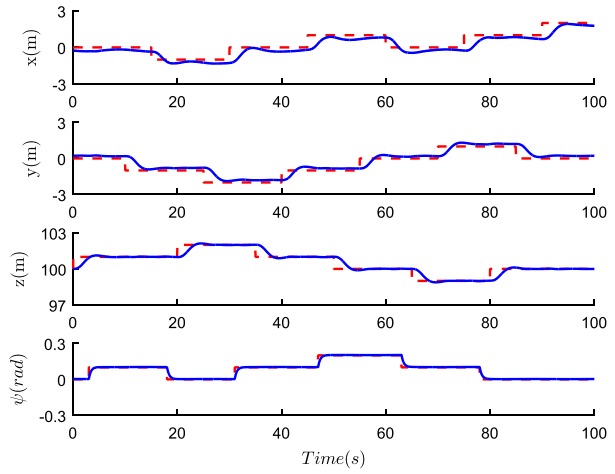

(a) System Outputs x, y, z and ψ (solid line) and the desired trajectories x_d, y_d, z_d and ψ_d (dashed line).

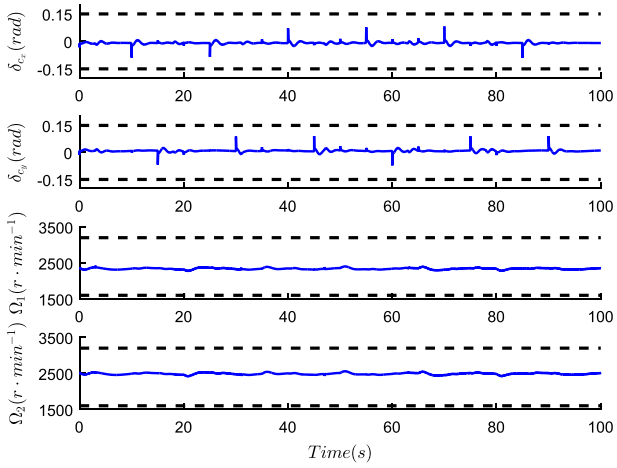

(b) Input signals δ_{c_x}, δ_{c_y}, Ω_1 and Ω_2 (solid line).

Fig. 4 Simulation result with sine-like external loads

trajectories even in the presence of unknown varying external loads. To testify the stability of the whole system, the control signals are also provided in Fig. 4b. Due to the involvement of unknown external loads, higher regulating frequency in the control inputs can be observed for compensating the additional disturbance.

4.3 Scenario 3: Flight with Sensing Noise

Moreover, considering that there always exists sensing noise in signal measurements, a numerical test similar to Scenario 2 but with measurement noise in output signals is conducted. Specifically, the system outputs (i.e., p, v, η and ω) are corrupted with 3% white noise. The generated trajectories depicted in Fig. 5a demonstrate alike tracking performance compared with Fig. 4a, even in the presence of sensing noise. Meanwhile, certain chattering phenomenon appears in the control signals plotted in Fig. 5b, which is a result of the high-frequency measurement noise.

4.4 Scenario 4: Flight with External Turbulent Disturbance

This simulation study is conducted by considering the fact that the stochastic winds are usually the major cause of external disturbance appearing in the flight of GLMAVs. In order to better imitate the actual flight, a turbulent wind is introduced into each body axis of the system dynamics via Eqs. 6 and 7. The wind is generated by Wind Turbine Blockset in Matlab Simulation based on the Kaimal turbulent model, whose profile is shown in Fig. 6. It has a mean value of $20m/s$ and turbulence intensity of 12%.

The simulation result in Fig. 7a shows satisfactory tracking performance of the controller despite of stochastic

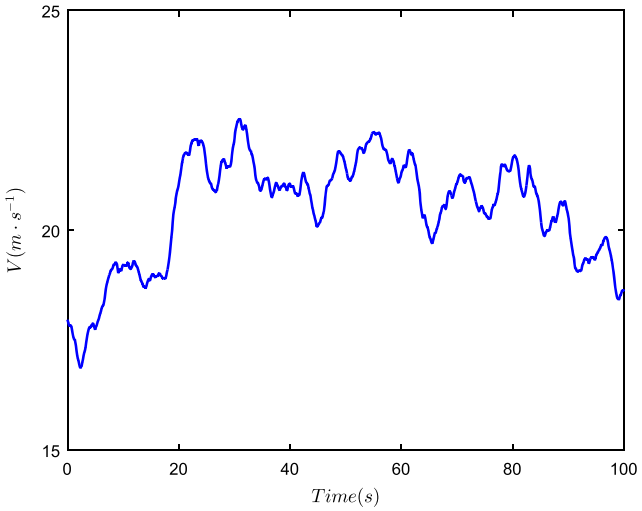

Fig. 6 Turbulent wind profile for scenario 3

turbulent winds. Fast convergence to the desired trajectory can be observed and the stability of the closed-loop system is further demonstrated in Fig. 7b. The proposed controller has exhibited strong robustness with respect to external disturbance in various conditions.

4.5 Scenario 5: Trajectory Tracking Comparison with Current Approaches

In this scenario, a comparison study between the proposed controller and the hierarchical approaches in [20, 21] is conducted for path tracking task under varying external loads adopted in Scenario 2. The output trajectories of all approaches are plotted in Figs. 8 and 9, respectively in 3D and top view. Although all of them can achieve satisfactory

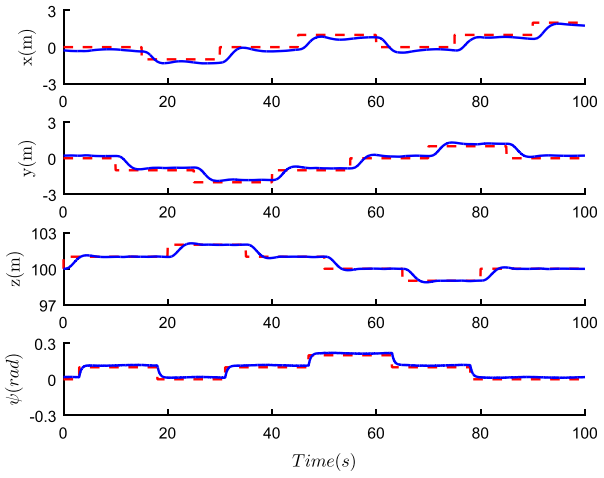

(a) System outputs x, y, z and ψ (solid line) and desired trajectories x_d, y_d, z_d and ψ_d (dashed line).

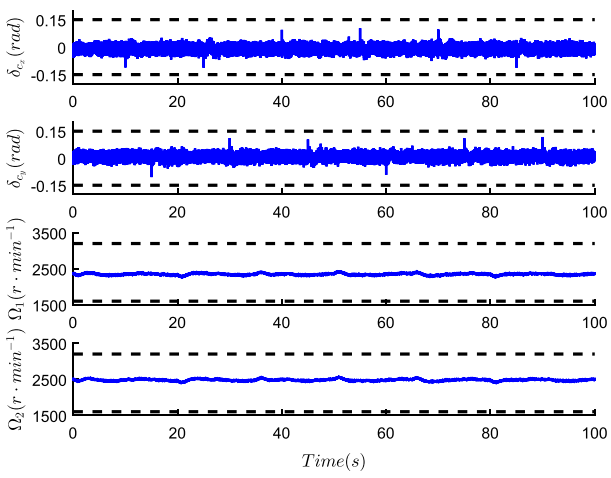

(b) Input signals δ_{c_x}, δ_{c_y}, Ω_1 and Ω_2 (solid line).

Fig. 5 Simulation result with sensing noise

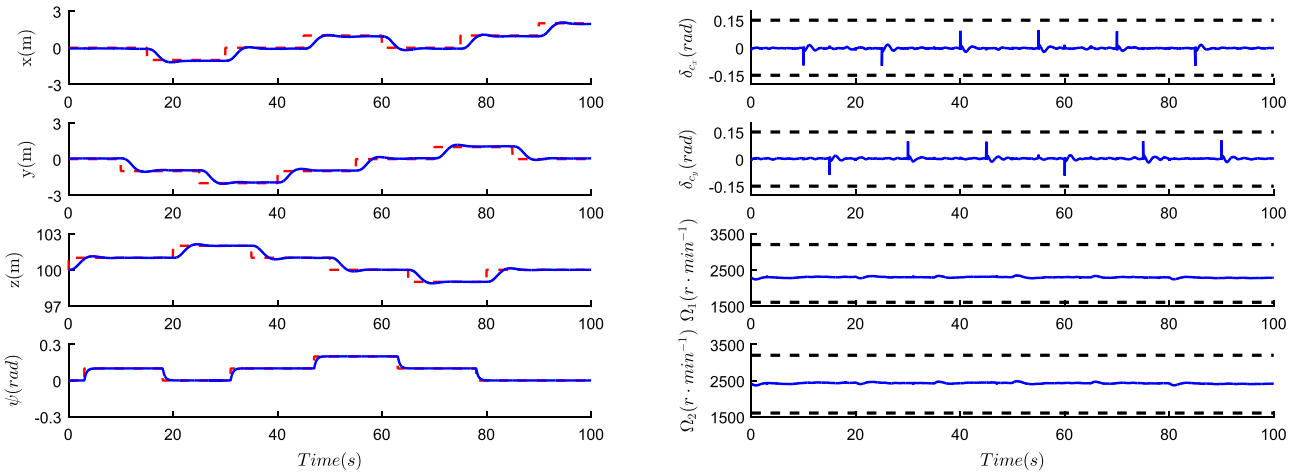

(a) System outputs x, y, z and ψ (solid line) and desired trajectories x_d, y_d, z_d and ψ_d (dashed line).

(b) Input signals δ_{c_x}, δ_{c_y}, Ω_1 and Ω_2 (solid line).

Fig. 7 Simulation result with external turbulent winds

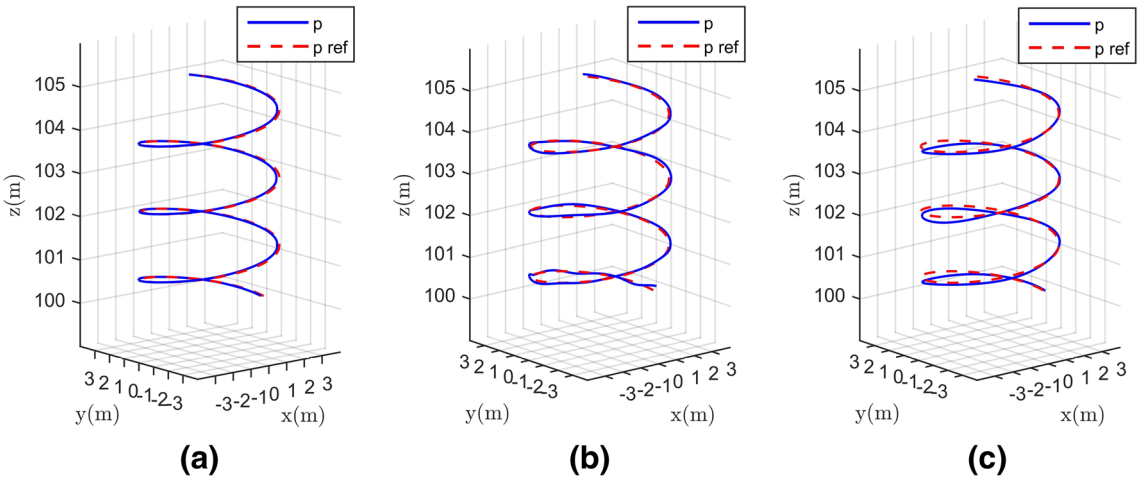

Fig. 8 Comparison result in 3D view (**a** the proposed approach; **b** controller with LESO in [20]; **c** controller with FTDO in [21])

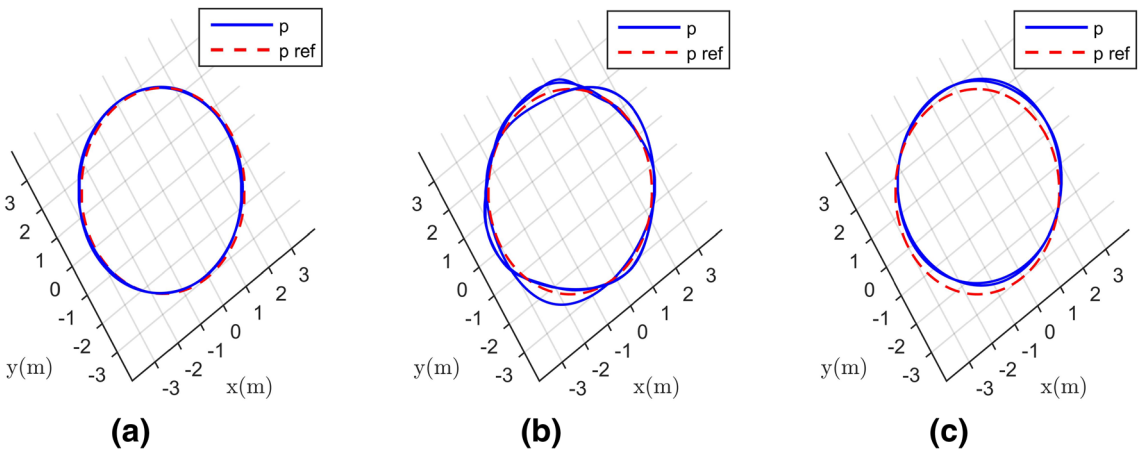

Fig. 9 Comparison result in top view (**a** the proposed approach; **b** controller with LESO in [20]; **c** controller with FTDO in [21])

tracking performance, it can be seen that the proposed controller delivers the best result.

5 Conclusion

In this paper, how to achieve satisfactory tracking control performance of an unmanned coaxial-rotor MAV in a highly uncertain environment is investigated. A detailed dynamic model with unknown external loads is firstly established for control design purpose. A nonlinear robust controller is then proposed based on filtered tracking errors and Lyapunov analysis provided that all system states are available. To overcome the practical challenge that certain states are not measurable, a high gain observer is introduced to estimate derivatives of the vehicle position and an output feedback controller is developed. Theoretical analysis verifies the stability of the entire closed-loop system. Additionally, extensive simulation studies illustrate that the proposed scheme can achieve a good performance in terms of position and orientation trajectory tracking.

Future work includes designing mechanical prototypes to conduct real-world experiments and proposing more intelligent control algorithms for the vehicle with severe system uncertainties (both external aerodynamic disturbances and undetermined system parameters).

Acknowledgements This work is supported by National Natural Science Foundation of China (Grant No. 61673347, U1609214).

Appendix

Proof of Theorem 1 Considering a candidate Lyapunov function

$$V = V_p + V_\psi \tag{48}$$

with

$$V_p = \frac{1}{2} r_p^T r_p, \quad V_\psi = \frac{1}{2} r_\psi^T r_\psi \tag{49}$$

Recalling Eq. 29, the time derivative of V_p is given by

$$\begin{aligned} \dot{V}_p &= r_p^T \dot{r}_p^T \\ &= -c_p r_p^T r_p + r_p^T \Phi_p - r_p^T \operatorname{sgn}(r_p)\, \Theta_p \\ &\le -c_p r_p^T r_p + |r_p^T| \Theta_p - r_p^T \operatorname{sgn}(r_p) \Theta_p \\ &\le -c_p r_p^T r_p \end{aligned} \tag{50}$$

Further, Eq. 32 can be employed to obtain the derivative of V_ψ

$$\begin{aligned} \dot{V}_\psi &= r_\psi^T \dot{r}_\psi^T \\ &= -c_\psi r_\psi^T r_\psi + r_\psi^T \Phi_\psi - r_\psi^T \operatorname{sgn}(r_\psi)\, \Theta_\psi \\ &\le -c_\psi r_\psi^T r_\psi + |r_\psi^T| \Theta_\psi - r_\psi^T \operatorname{sgn}(r_\psi)\, \Theta_\psi \\ &\le -c_\psi r_\psi^T r_\psi \end{aligned} \tag{51}$$

Thus, the derivative of V is

$$\dot{V} = \dot{V}_p + \dot{V}_\psi \le -c_\psi r_\psi^T r_\psi - c_p r_p^T r_p \le cV \tag{52}$$

where $c = \min\{2c_p, 2c_\psi\}$. Solving Eq. 52 generates

$$0 \le V \le V(0) e^{-ct} \tag{53}$$

where $V(0) = \frac{1}{2}(r_p^T(0) r_p(0) + r_\psi^T(0) r_\psi(0))$ is the initial value.

Obviously, $V \to 0$ as $t \to \infty$. This implies that $r_p, r_\psi \to 0$ as $t \to \infty$. Subsequently, the tracking error δ_{p_i} and δ_{ψ_i} defined in Eqs. 16 and 23 also converge to zero asymptotically by definition. Thus, the closed-loop system can asymptotically track the reference trajectories p_d and ψ_d. With the help of Eq. 18 and Assumption $1-2$, v and T_z are bounded. R_η and Q_η are also bounded since $-\frac{\pi}{2} < \theta, \phi < \frac{\pi}{2}$. Similarly, the signals ω_x, ω_y and $\dot{T}_z$ are all bounded according to Eq. 18. Through Eq. 25, one can reach that ω_z is bounded, and so is $\dot{Q}_\eta$. Thus, the two control inputs τ and $\ddot{T}_z$ are also bounded from Eq. 33. □

Proof of Theorem 2 Consider the following Lyapunov function candidate

$$\overline{V} = \overline{V}_p + \overline{V}_\psi \tag{54}$$

with

$$\overline{V}_p = \frac{1}{2} r_p^T r_p + e_p^T P e_p, \quad \overline{V}_\psi = \frac{1}{2} r_\psi^T r_\psi \tag{55}$$

Define the estimated filtered position tracking error as

$$\hat{r}_p = k_{p0}\delta_{p0} + k_{p1}\delta_{p1} + k_{p2}\hat{\delta}_{p2} + \hat{\delta}_{p3} \tag{56}$$

If enforcing the output feedback controller (45), the filtered position tracking error dynamics (27) can be rewritten as

$$\begin{aligned} \dot{r}_p &= -\tanh\left(\frac{\hat{r}_p}{\varepsilon_p}\right) \Theta_p + \Phi_p + k_{p0}\delta_{p1} + k_{p1}\delta_{p2} \\ &\quad + k_{p2}\delta_{p3} - c_p \hat{r}_p - \left(k_{p0}\delta_{p1} + k_{p1}\hat{\delta}_{p2} + k_{p2}\hat{\delta}_{p3}\right) \\ &= -\tanh\left(\frac{\hat{r}_p}{\varepsilon_p}\right) \Theta_p + \Phi_p + (k_{p1} + c_p k_{p2}) e_{p2} \\ &\quad + (k_{p2} + c_p) e_{p3} - c_p r_p \end{aligned} \tag{57}$$

Thus, the derivative of $\overline{V}_p$ can be given by

$$\begin{aligned} \dot{\overline{V}}_p &= r_p^T \dot{r}_p + \dot{e}_p^T P e_p + e_p^T P \dot{e}_p \\ &= -r_p^T \tanh\left(\frac{\hat{r}_p}{\varepsilon_p}\right) \Theta_p + r_p^T \Phi_p + (k_{p1} + c_p k_{p2}) r_p^T e_{p2} \\ &\quad + (k_{p2} + c_p) r_p^T e_{p3} - c_p r_p^T r_p + \dot{e}_p^T P e_p + e_p^T P \dot{e}_p \end{aligned} \tag{58}$$

Substituting Eqs. 40 and 42 into Eq. 58 generates

$$\begin{aligned}\dot{\overline{V}}_p &= -r_p^T \tanh\left(\frac{\hat{r}_p}{\varepsilon_p}\right)\Theta_p + r_p^T\Phi_p - c_p r_p^T r_p \\ &\quad +(k_{p_1}+c_p k_{p_2})r_p^T e_{p_2} + (k_{p_2}+c_p)r_p^T e_{p_3} \\ &\quad +e_p^T(A^T P + PA)e_p + 2e_p^T PB\Phi_p \\ &= -r_p^T \tanh\left(\frac{\hat{r}_p}{\varepsilon_p}\right)\Theta_p + r_p^T\Phi_p - c_p r_p^T r_p \\ &\quad +(k_{p_1}+c_p k_{p_2})r_p^T e_{p_2} + (k_{p_2}+c_p)r_p^T e_{p_3} \\ &\quad -\lambda e_p^T e_p + 2e_p^T PB\Phi_p\end{aligned} \tag{59}$$

Meanwhile, by resorting to Lemma 1, it is apparent that for the vector $r_p \in \mathbb{R}^3$ and a positive constant $\varepsilon_p > 0$,

$$\begin{aligned}0 &\le r_p^T\left(\mathrm{sgn}(r_p) - \tanh\left(\frac{r_p}{\varepsilon_p}\right)\right) \\ &= |r_p| - r_p^T \tanh\left(\frac{r_p}{\varepsilon_p}\right) \le 3\kappa\varepsilon_p\end{aligned} \tag{60}$$

Thus, one further has

$$\begin{aligned}\dot{\overline{V}}_p &= -r_p^T \tanh\left(\frac{\hat{r}_p}{\varepsilon_p}\right)\Theta_p + r_p^T \tanh\left(\frac{r_p}{\varepsilon_p}\right)\Theta_p \\ &\quad -r_p^T \tanh\left(\frac{r_p}{\varepsilon_p}\right)\Theta_p + r_p^T \mathrm{sgn}\left(r_p\right)\Theta_p \\ &\quad -r_p^T \mathrm{sgn}\left(r_p\right)\Theta_p + r_p^T\Phi_p - c_p r_p^T r_p \\ &\quad +(k_{p_1}+c_p k_{p_2})r_p^T e_{p_2} + (k_{p_2}+c_p)r_p^T e_{p_3} \\ &\quad -\lambda e_p^T e_p + 2e_p^T PB\Phi_p \\ &\le -r_p^T \tanh\left(\frac{\hat{r}_p}{\varepsilon_p}\right)\Theta_p + r_p^T \tanh\left(\frac{r_p}{\varepsilon_p}\right)\Theta_p \\ &\quad +3\kappa\varepsilon_p\Theta_p - r_p^T \mathrm{sgn}\left(r_p\right)\Theta_p + r_p^T\Phi_p - c_p r_p^T r_p \\ &\quad +(k_{p_1}+c_p k_{p_2})r_p^T e_{p_2} + (k_{p_2}+c_p)r_p^T e_{p_3} \\ &\quad -\lambda e_p^T e_p + 2e_p^T PB\Phi_p \\ &\le 3\kappa\varepsilon_p\Theta_p + r_p^T\left(\tanh\left(\frac{r_p}{\varepsilon_p}\right) - \tanh\left(\frac{\hat{r}_p}{\varepsilon_p}\right)\right)\Theta_p \\ &\quad (k_{p_1}+c_p k_{p_2})r_p^T e_{p_2} + (k_{p_2}+c_p)r_p^T e_{p_3} \\ &\quad -c_p r_p^T r_p - \lambda e_p^T e_p + 2e_p^T PB\Phi_p\end{aligned} \tag{61}$$

With the help of Young's inequality and the fact that $|\tanh(\cdot)| \le 1$, Eq. 61 results in

$$\begin{aligned}\dot{\overline{V}}_p &\le 3\kappa\varepsilon_p\Theta_p + \frac{r_p^T r_p}{2\varepsilon_1} + 6\varepsilon_1\Theta_p^2 - c_p r_p^T r_p \\ &\quad +\left(k_{p_1}+c_p k_{p_2}\right)\left(\frac{r_p^T r_p}{2\varepsilon_2} + \frac{\varepsilon_2 e_{p_2}^T e_{p_2}}{2}\right) \\ &\quad +(k_{p_2}+c_p)\left(\frac{r_p^T r_p}{2\varepsilon_3} + \frac{\varepsilon_3 e_{p_3}^T e_{p_3}}{2}\right) - \lambda e_p^T e_p \\ &\quad +\varepsilon_4 e_p^T e_p + \frac{\|PB\Phi_p\|^2}{\varepsilon_4} \\ &\le -\left(c_p - \frac{1}{2\varepsilon_1} - \frac{k_{p_1}+c_p k_{p_2}}{2\varepsilon_2} - \frac{k_{p_2}+c_p}{2\varepsilon_3}\right) r_p{}^T r_p \\ &\quad -\left(\lambda - \frac{(k_{p_1}+c_p k_{p_2})\varepsilon_2}{2} - \frac{(k_{p_2}+c_p)\varepsilon_3}{2} - \varepsilon_4\right) e_p^T e_p \\ &\quad +3\kappa\varepsilon_p\Theta_p + 6\varepsilon_1\Theta_p^2 + \frac{\|PB\Phi_p\|^2}{\varepsilon_4}\end{aligned} \tag{62}$$

where $\|\cdot\|$ denotes the L_2-norm, and $\varepsilon, \varepsilon_1, \varepsilon_2, \varepsilon_3, \varepsilon_4 \in \mathbb{R}^+$.

Similarly, with the controlled designed in Eq. 45, the filtered orientation tracking error dynamics can be rephrased to be

$$\dot{r}_\psi = -c_\psi r_\psi - \tanh\left(\frac{r_\psi}{\varepsilon_\psi}\right)\Theta_\psi + \Phi_\psi \tag{63}$$

Hence, the derivative of $\overline{V}_\psi$ can be given by

$$\begin{aligned}\dot{\overline{V}}_\psi &= r_\psi^T \dot{r}_\psi = -r_\psi^T \tanh\left(\frac{r_\psi}{\varepsilon_\psi}\right)\Theta_\psi + r_\psi^T\Phi_\psi - c_\psi r_\psi^T r_\psi \\ &\le -c_\psi r_\psi^T r_\psi + \kappa\varepsilon_\psi\Theta_\psi\end{aligned} \tag{64}$$

Combining Eq. 62 with Eq. 64 delivers

$$\begin{aligned}\dot{\overline{V}} &\le -\left(c_p - \frac{1}{2\varepsilon_1} - \frac{k_{p_1}+c_p k_{p_2}}{2\varepsilon_2} - \frac{k_{p_2}+c_p}{2\varepsilon_3}\right) r_p{}^T r_p \\ &\quad -\left(\lambda - \frac{(k_{p_1}+c_p k_{p_2})\varepsilon_2}{2} - \frac{(k_{p_2}+c_p)\varepsilon_3}{2} - \varepsilon_4\right) e_p^T e_p \\ &\quad -c_\psi r_\psi^T r_\psi + \kappa\left(3\varepsilon_p\Theta_p + \varepsilon_\psi\Theta_\psi\right) + 6\varepsilon_1\Theta_p^2 + \frac{\|PB\Phi_p\|^2}{\varepsilon_4} \\ &\le -c_{p_1} r_p{}^T r_p - c_{p_2} e_p^T e_p - c_\psi r_\psi^T r_\psi + C\end{aligned} \tag{65}$$

where $c_{p_1}, c_{p_2}, C \in \mathbb{R}^+$ with

$$\begin{aligned}c_{p_1} &= c_p - \frac{1}{2\varepsilon_1} - \frac{k_{p_1}+c_p k_{p_2}}{2\varepsilon_2} - \frac{k_{p_2}+c_p}{2\varepsilon_3} \\ c_{p_2} &= \lambda - \frac{(k_{p_1}+c_p k_{p_2})\varepsilon_2}{2} - \frac{(k_{p_2}+c_p)\varepsilon_3}{2} - \varepsilon_4 \\ C &= \kappa\left(3\varepsilon_p\Theta_p + \varepsilon_\psi\Theta_\psi\right) + 6\varepsilon_1\Theta_p^2 + \frac{\|PB\Phi_p\|^2}{\varepsilon_4}\end{aligned} \tag{66}$$

Hence, $\dot{\overline{V}}$ will becomes negative as long as

$$r_p \notin \Omega_{r_p} = \left\{ r_p \,\middle|\, \|r_p\| \le \sqrt{\frac{C}{c_{p_1}}} \right\} \tag{67}$$

or

$$e_p \notin \Omega_{e_p} = \left\{ e_p \,\middle|\, \|e_p\| \le \sqrt{\frac{C}{c_{p_2}}} \right\} \tag{68}$$

or

$$r_\psi \notin \Omega_{r_\psi} = \left\{ r_\psi \,\middle|\, \|r_\psi\| \le \sqrt{\frac{C}{c_\psi}} \right\} \tag{69}$$

According to the standard Lyapunov analysis, one has that the filtered tracking errors r_p, r_ψ, and the observer error e_p are uniformly ultimately bounded (UUB). Furthermore, the tracking errors can be arbitrarily reduced by increasing control gains c_ψ, c_p, h_1, h_2 and h_3. By following the similar analysis in Proof of Theorem 1, the signals T_z, $\dot{T}_z$, ω are bounded as well as all the elements of R_η, Q_η and $\dot{Q}_\eta$. Furthermore, the estimation signals $\hat{\delta}_{p_2}$, $\hat{\delta}_{p_3}$ and $\hat{r}_p$ are bounded since the observer error vector e_p is bounded. Thus, the control signals $\ddot{T}_z$ and τ are proved to be bounded from Eq. 45. □

References

1. Anderson, B., Fidan, B., Yu, C., Walle, D.: Uav formation control: theory and application. Recent Advan. Learn. Control **371**, 15–33 (2008)
2. Basri, M.A.M., Husain, A.R., Danapalasingam, K.A.: Enhanced backstepping controller design with application to autonomous quadrotor unmanned aerial vehicle. J. Intell. Robot. Syst. **79**(2), 295 (2015)

3. Drouot, A., Richard, E., Boutayeb, M.: Nonlinear backstepping based trajectory tracking control of a gun launched micro aerial vehicle. In: AIAA Guidance, Navigation, and Control Conference, p. 4455 (2012)
4. Drouot, A., Richard, E., Boutayeb, M.: An approximate backstepping based trajectory tracking control of a gun launched micro aerial vehicle in crosswind. J. Intell. Robot. Syst. **1**(70), 133–150 (2013)
5. Drouot, A., Richard, E., Boutayeb, M.: Hierarchical backstepping-based control of a gun launched mav in crosswinds: theory and experiment. Control. Eng. Pract. **25**, 16–25 (2014)
6. Gnemmi, P., Haertig, J.: Concept of a gun launched micro air vehicle. In: 26Th AIAA Applied Aerodynamics Conference, p. 6743 (2008)
7. Gnemmi, P., Koehl, A., Martinez, B., Changey, S., Theodoulis, S.: Modeling and control of two glmav hover-flight concepts. In: Proceedings of the European Micro Aerial Vehicle Conference (2009)
8. Hausamann, D., Zirnig, W., Schreier, G., Strobl, P.: Monitoring of gas pipelines–a civil uav application. Aircraft Eng. Aerospace Technol. **77**(5), 352–360 (2005)
9. Keller, J., Thakur, D., Dobrokhodov, V., Jones, K., Pivtoraiko, M., Gallier, J., Kaminer, I., Kumar, V.: A computationally efficient approach to trajectory management for coordinated aerial surveillance. Unmanned Syst. **1**(01), 59–74 (2013)
10. Kendoul, F.: Survey of advances in guidance, navigation, and control of unmanned rotorcraft systems. J. Field Rob. **29**(2), 315–378 (2012)
11. Kendoul, F., Yu, Z., Nonami, K.: Guidance and nonlinear control system for autonomous flight of minirotorcraft unmanned aerial vehicles. J. Field Rob. **27**(3), 311–334 (2010)
12. Koehl, A., Boutayeb, M., Rafaralahy, H., Martinez, B.: wind-disturbance and aerodynamic parameter estimation of an experimental launched micro air vehicle using an Ekf-like observer. In: 2010 49th IEEE Conference on Decision and Control (CDC), pp. 6383–6388. IEEE (2010)
13. Koehl, A., Rafaralahy, H., Boutayeb, M., Martinez, B.: Time-varying observers for launched unmanned aerial vehicle. IFAC Proc. **44**(1), 14,380–14,385 (2011)
14. Koehl, A., Rafaralahy, H., Boutayeb, M., Martinez, B.: Aerodynamic modelling and experimental identification of a coaxial-rotor uav. J. Intell. Robot. Syst. **68**(1), 53–68 (2012)
15. Koehl, A., Rafaralahy, H., Martinez, B., Boutayeb, M.: Modeling and identification of a launched micro air vehicle: design and experimental results. In: AIAA Modeling and Simulation Technologies Conference (2010)
16. Kumar, V., Michael, N.: Opportunities and challenges with autonomous micro aerial vehicles. Int. J. Robot. Res. **31**(11), 1279–1291 (2012)
17. Mahony, R., Hamel, T.: Robust trajectory tracking for a scale model autonomous helicopter. Int. J. Robust Nonlinear Control **14**(12), 1035–1059 (2004)
18. McCormick, B.W.: Aerodynamics, Aeronautics, and Flight Mechanics, vol. 2. Wiley, New York (1995)
19. Meng, W., Yang, Q., Jagannathan, S., Sun, Y.: Adaptive neural control of high-order uncertain nonaffine systems: a transformation to affine systems approach. Automatica **50**(5), 1473–1480 (2014)
20. Mokhtari, M.R., Braham, A.C., Cherki, B.: Extended state observer based control for coaxial-rotor uav. ISA Trans. **61**, 1–14 (2016)
21. Mokhtari, M.R., Cherki, B., Braham, A.C.: Disturbance observer based hierarchical control of coaxial-rotor uav. ISA Trans. **67**, 466–475 (2017)
22. Nonami, K.: Prospect and recent research & development for civil use autonomous unmanned aircraft as uav and mav. J. syst. Des. Dyn. **1**(2), 120–128 (2007)
23. Nonami, K., Kendoul, F., Suzuki, S., Wang, W., Nakazawa, D.: Autonomous Flying Robots: Unmanned Aerial Vehicles and Micro Aerial Vehicles. Springer, Berlin (2010)
24. Pflimlin, J.M., Souères, P., Hamel, T.: Position control of a ducted fan vtol uav in crosswind. Int. J. Control. **80**(5), 666–683 (2007)
25. Pines, D.J., Bohorquez, F.: Challenges facing future micro-air-vehicle development. J. Aircr. **43**(2), 290–305 (2006)
26. Polycarpou, M.M., Ioannou, P.A.: A robust adaptive nonlinear control design. Automatica **32**(3), 423–427 (1996)
27. Schroeder, D.J.: Astronomical Optics. Academic Press, Cambridge (1999)
28. Sepulchre, R., Jankovic, M., Kokotovic, P.V.: Constructive Nonlinear Control. Springer, Berlin (2012)
29. Teel, A.R.: A nonlinear small gain theorem for the analysis of control systems with saturation. IEEE Trans. Autom. Control **41**(9), 1256–1270 (1996)
30. Wood, R.J., Avadhanula, S., Steltz, E., Seeman, M., Entwistle, J., Bachrach, A., Barrows, G., Sanders, S.: An autonomous palm-sized gliding micro air vehicle. IEEE Robot. Autom. Mag. **14**(2), 82–91 (2007)
31. Yang, Q., Yang, Z., Sun, Y.: Universal neural network control of mimo uncertain nonlinear systems. IEEE Trans. Neural Netw. Learn. Syst. **23**(7), 1163–1169 (2012)

Jinglan Li received the Bachelor's degree in Automation from the Zhejiang University,Hangzhou, China in 2015. He is currently working toward the Ph.D. degree in Control Science and Engineering at Zhejiang University, Hangzhou, China. He is a member of the Group of Networked Sensing and Control (IIPC-NeSC), State Key Laboratory of Industrial Control Technology, Zhejiang University. His research interests include nonlinear system theory and robotics.

Qinmin Yang received the Bachelor's degree in Electrical Engineering from Civil Aviation University of China, Tianjin, China in 2001, the Master of Science Degree in Control Science and Engineering from Institute of Automation, Chinese Academy of Sciences, Beijing, China in 2004, and the Ph.D. degree in Electrical Engineering from the University of Missouri-Rolla, MO USA, in 2007. From 2007 to 2008, he was a Post-doctoral Research Associate at University of Missouri-Rolla. In 2008, he was a system engineer with Caterpillar Inc. From 2009 to 2010, he was a Post-doctoral Research Associate at University of Connecticut. Since 2010, he has been with the State Key Laboratory of Industrial Control Technology, the Department of Control Science and Engineering, Zhejiang University, China, where he is currently a full professor. His research interests include intelligent control, renewable energy systems, nano-robotics, and system diagnosis.

Youxian Sun received the Diploma degree from the Department of Chemical Engineering, Zhejiang University, Hangzhou, China, in 1964. His current research interests include the modeling, control, and optimization of complex systems and robust control design and its applications.In 1964, he joined the Department of Chemical Engineering, Zhejiang University. From 1984 to 1987, he was an Alexander Von Humboldt Research Fellow, and Visiting Associate Professor with the University of Stuttgart, Stuttgart, Germany. Since 1988, he has been a Full Professor with Zhejiang University. For his distinguished contributions to automatic control technology and industrial automation, he was elevated to an Academician of the Chinese Academy of Engineering in 1995. He is the author or coauthor of 18 books and more than 500 journal and conference proceeding papers. He is currently the Director of the Institute of Industrial Process Control and the National Engineering Research Center of Industrial Automation, Zhejiang University. He serves as the President of Chinese Association of Automation, and also served as Vice-Chairman of IFAC Pulp and Paper Committee, and Vice-President of the China Instrument and Control Society. He is a Fellow of IFAC.